7

Planetary fields and dynamos

Ulrich R. Christensen

7.1 Introduction

Over four centuries ago it was realized that the time-averaged direction of a compass needle is not affected by a force emanating from the sky, but by a magnetic field that is intrinsic to the Earth. The basic structure of the geomagnetic field and its slow variation with time was characterized long before magnetic fields were detected on other celestial bodies. By the middle of the twentieth century, the study of remanent magnetization of natural rocks had firmly established that the principal dipole component of the Earth's magnetic field had reversed its direction many times in the past.

Our understanding of the origin of the field by a dynamo process in the Earth's core has developed at a much slower pace, basically in parallel with that of astrophysical dynamos in general. Aside from understanding the intricate details of how a magnetic field is generated by a dynamo, we must ascertain that some fundamental requirements are fulfilled inside our planet. Geophysical observations have shown that one condition, namely the existence of an electrically conducting fluid region, is met inside the Earth, which has an outer core consisting of a liquid iron alloy. It is likely, but not completely certain, that all big planets have conducting fluid cores (see Fig. 7.5). However, some planets may not conform with another basic condition for a dynamo, namely sufficiently fast motion in the fluid layer. Convection is envisaged as the most likely source of a flow that can sustain a dynamo, but in some planets the fluid core may be stably stratified.

Since 1995, numerical modeling of the geodynamo has been thriving. Global models of convection-driven dynamos in a rotating spherical shell show magnetic fields that resemble the geomagnetic field in many respects – they are dominated by the axial dipole of approximately the right strength, they show spatial power spectra similar to that of Earth's magnetic field, and the magnetic field morphology and the temporal variation of the field resembles that of the geomagnetic field. While

Heliophysics: Evolving Solar Activity and the Climates of Space and Earth, eds. Carolus J. Schrijver and George L. Siscoe. Published by Cambridge University Press.

these models represent direct numerical simulations of the fundamental magnetohydrodynamic equations without parameterized induction effects, they do not match actual planetary conditions in a number of respects and their success appears somewhat surprising.

Space missions revealed that most planets in the solar system have internal magnetic fields (see Vol. I, Chapter 13), but there are exceptions (Venus, Mars). Some planets seem to have had a field that is now extinguished (e.g. Mars). In many cases with an active dynamo the axial dipole dominates the field at the planetary surface (Fig. 13.2 in Vol. I), but Uranus and Neptune are exceptions. Saturn is special because its field is extremely symmetric with respect to the planet's rotation axis. The field strengths at the planetary surfaces differ by a factor of 1000 between Mercury and Jupiter. A full understanding of this diversity in the morphology and strength of planetary magnetic fields is still lacking, but a number of promising ideas have been suggested and backed up by dynamo simulations. Some of the differences can be explained by a systematic dependence of the dynamo behavior on parameters such as rotation rate or energy flux, whereas others seem to require qualitative differences in the structure and dynamics of the planetary dynamos.

This chapter summarizes our state of knowledge about the structure and time dependence of the geomagnetic field and the more limited knowledge on the fields of other planets. The internal constitution and the thermal budget of the planets is discussed as far as it is essential for the understanding of planetary dynamos. The fundamentals of astrophysical dynamos have been described in Chapters 5 and 6, and in Vol. I, Chapter 3; here we discuss conditions for fluid flow and magnetic field generation that are particular to planetary cores and we contrast them with those in the Sun. We give special consideration to numerical simulations that have played a major role in our understanding of the generation of planetary magnetic fields.

7.2 Geomagnetic field

7.2.1 Field structure

For the last four hundred years the Earth's magnetic field has been mapped sufficiently well to determine its global structure. Most of the early measurements were taken routinely by mariners (Jackson *et al.*, 2000). Usually only the declination was recorded, i.e. the deviation of the horizontal component of the magnetic field from true north. Other measurements have been taken for scientific reasons and included the inclination, i.e. the angle between the field direction and Earth's surface. In 1832, Carl Friedrich Gauss developed a method that allowed the intensity of the field to be measured in absolute terms for the first time. Not much later the first permanent magnetic observatories were established.

Gauss was also the first to realize that the magnetic field **B** near the Earth's surface (and in general in a source-free region) can be represented as the gradient of a scalar potential Φ. He introduced the presentation of the field in terms of spherical harmonic functions and Gauss coefficients g_n^m and h_n^m, as they are now called:

$$\Phi = R_\mathrm{p} \sum_{n=1}^{\infty} \sum_{m=0}^{n} \left(\frac{R_\mathrm{p}}{r}\right)^{n+1} P_n^m(\cos\theta) \left(g_n^m \cos m\lambda + h_n^m \sin m\lambda\right), \qquad (7.1)$$

where r is the distance from the planet's center, R_p is the (equatorial) radius of the planet, θ is the co-latitude, λ longitude, n and m are spherical harmonic degree and order, respectively, and P_n^m are the associated Legendre functions in the so-called Schmidt normalization. g_1^0 describes the axial dipole ("axial" means aligned with the planet's rotation axis), g_1^1 and h_1^1 the equatorial dipole, terms with $n = 2$ the quadrupole, those with $n = 3$ the octupole, and so on. Equation (7.1) is formulated such that the coefficients g and h have the unit of magnetic induction (here also called magnetic field strength). Usually the sub-unit nanotesla (nT) is used in geophysics and planetary sciences (100 000 nT = 1 gauss).

Often a characterization of the magnetic field of planets other than Earth in terms of a dipole that is offset from the planet's center can be found in the literature. This is an outdated description, because it is very implausible that the dynamo region is not spherically symmetric with respect to the planet's center of mass. A combination of a planetocentric dipole and higher multipoles is equivalent to an off-center dipole.

The complete description of a potential field requires additional terms in Eq. (7.1) that vary with radius as $(r/R_\mathrm{p})^{n-1}$. These terms describe a field component of external (ionospheric or magnetospheric) origin. Gauss found that for the Earth they are small in comparison to those describing an internal field (see Section 7.3 for the impact on measurements of fields from other planets using spacecraft flybys).

The properties of the recent geomagnetic field have been mapped with high spatial resolution by dedicated satellite missions carrying magnetometers in a low-Earth orbit, namely MAGSAT in 1980, and ØRSTED and CHAMP since 1999 and 2000, respectively (Olsen *et al.*, 2007). Spherical harmonic representations of the Earth's internal magnetic field up to degree and order 100 are available. When aiming at an understanding of the geodynamo, it is more meaningful to consider the magnetic field structure at the surface of the core, within which the dynamo process operates, rather than at the Earth's surface. To the extent that there are no significant sources of the magnetic field in the Earth's crust and mantle (made of silicate rock), Eq. (7.1) can be used to downward continue the magnetic field from $r \approx R_\mathrm{p}$, where it is observed, to the core surface at R_c. In Fig. 7.1 spatial power

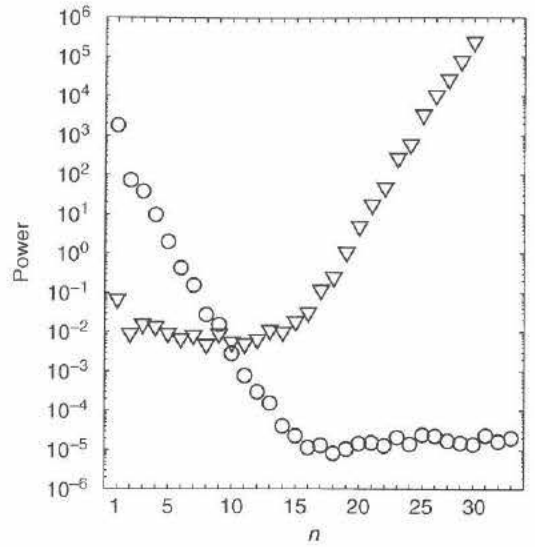

Fig. 7.1. Spatial power spectra of the geomagnetic field in 2004 according to the POMME model (Maus *et al.*, 2006) as function of spherical harmonic degree n at Earth's surface (circles) and at the core–mantle boundary (triangles; offset in amplitude). Note that structures of the core field corresponding to $n > 13$ are veiled by the crustal magnetic field, and that the apparent rise in the power spectrum does not reveal the properties of the deep geomagnetic field. Units are μT^2 for the surface field and mT^2 for the core field.

spectra of the magnetic field are compared for the Earth's surface (circles) and the core–mantle boundary (triangles). The degree power at radius r is given by

$$P_n = (n+1)\left(\frac{R_p}{r}\right)^{2n+4} \sum_{m=0}^{n} \left(\left(g_n^m\right)^2 + \left(h_n^m\right)^2\right). \tag{7.2}$$

The spectrum at Earth's surface drops sharply up to spherical harmonic degree 13, and is nearly white beyond that. The spectrum of the field projected onto the core–mantle boundary is almost white up to $n = 13$, except for the dipole term, which stands out by a factor between five and ten. For $n > 13$ the spectrum rises steeply, which is considered to be a very unlikely property of the core field. The generally accepted interpretation of these spectra is that the field at the Earth's surface is dominated by the core field at large scales up to $n \approx 13$. At shorter scales the geometric attenuation of the core field with radius is very strong (Eq. 7.1). The relatively weak magnetic field due to the inhomogeneous remanent and induced magnetization of small amounts of ferromagnetic minerals in the Earth's crust takes over and dominates the observed surface field. Projecting this small-scale field onto the core–mantle boundary is unphysical and leads to the blue spectrum for $n > 13$. As a consequence, we know the magnetic field at the surface of Earth's core only at

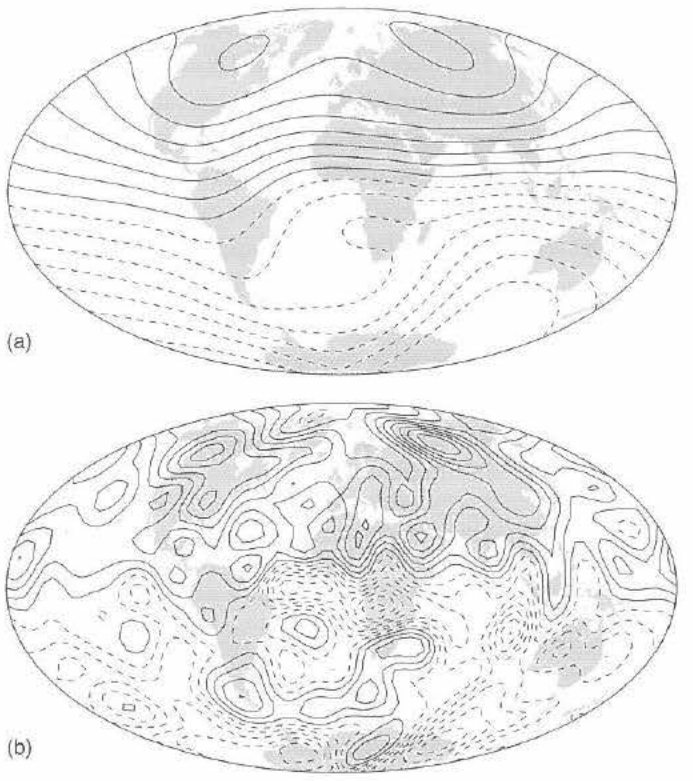

Fig. 7.2. Radial component of the geomagnetic field at the Earth's surface (a) and at the core–mantle boundary (b). Full lines for inward magnetic flux and dashed lines for outward flux. Contour intervals are arbitrary and different in the two panels.

large and intermediate wavelengths. Structures of the core field corresponding to $n > 13$ are veiled by the crustal magnetic field. The fine structure at the top of the solar dynamo is much better resolved than that of the geodynamo.

Figure 7.2 shows the radial component of the geomagnetic field at the Earth's surface (panel a) and, truncated at $n = 13$, at the core–mantle boundary (panel b). At the surface, the dipole part is very dominant. At the core–mantle boundary, in contrast, the dipole dominance is still visible, but there is significant structure at smaller scales. Most of the dipole field is formed by strong concentrations of magnetic flux into four lobes, two in each hemisphere, centered at $\pm(60°–70°)$ latitude. The prominent flux lobes in the Northern Hemisphere, under North America and Siberia, have counterparts in the Southern Hemisphere that lie at approximately the same longitudes. Close to the rotation poles, the flux is weak or even inverse with respect to the dominant polarity of the respective hemisphere. Patches of magnetic flux of both polarities are found at low and mid-latitudes.

The rms magnetic field strength at the core–mantle boundary is 0.39 mT in harmonic degrees from 1 to 13. It is uncertain how much components with $n > 13$ add; possibly they might double the mean strength. The mean field strength inside the dynamo is even more difficult to estimate. Speculations that the toroidal magnetic field in the Earth's core would be much stronger than the poloidal magnetic field, as it likely is in the Sun, are not supported by geodynamo models. A range of 1–4 mT (10–40 G) seems plausible for the internal field strength of the geodynamo.

Figure 7.2 represents a snapshot of a time-dependent magnetic field. Maps of the core field based on the historical record of observations have been constructed back until the year 1590, although with degrading spatial resolution (Jackson *et al.*, 2000, 2007). Although the details of the field structure change, some general traits seem to remain the same. The Northern Hemisphere flux lobes, in particular, are persistent and stay more or less in place.

7.2.2 Time-variability of Earth's field and the paleofield

The Earth's internal magnetic field changes on various time scales ranging from one year to a hundred million years. The changes that occurred during the past 400 years are documented by direct measurements. Going further back in time is possible by accessing the huge archive of magnetized rocks, which date back to various epochs of geological time and which recorded the magnetic field at the time of their formation.

7.2.2.1 Secular variation

The non-axial dipole part of the Earth's field, comprising the equatorial dipole and higher multipoles, changes significantly over a century. This is called the geomagnetic secular variation. Even in the eighteenth century it was noticed that part of the variation can be described as a westward drift of magnetic structures. The axial dipole changes more slowly; since 1840 the dipole moment has decreased by about 9%.

Much more recently, the magnetic field changes at the core–mantle boundary have been used to infer the flow of liquid iron at the top of Earth's core. This is based on the assumption that on the decadal time scale the magnetic flux is approximately frozen into the moving fluid (Alfvén's theorem, see Vol. I, Section 3.2.3.1). This alone is not sufficient to invert the field changes uniquely for the pattern of the large-scale flow and additional assumptions must be made (Holme, 2007). Figure 7.3 shows an example for a map of the core flow; other maps are broadly similar. The predominantly westward flow associated with the westward magnetic drift is restricted to the Atlantic hemisphere of the globe (where the westward drift

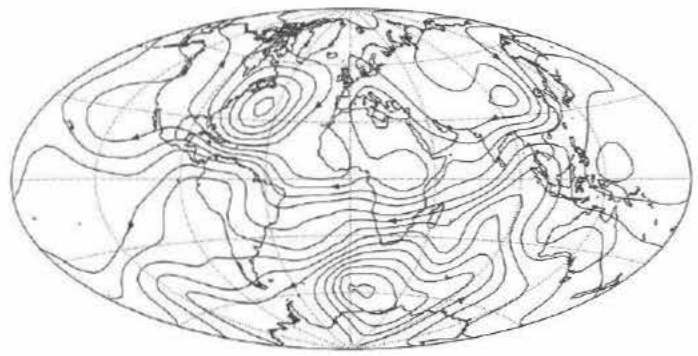

Fig. 7.3. Streamlines of the flow at the surface of the Earth's core inferred from the geomagnetic secular variation under the frozen flux assumption for the year 1980. (Adapted from Amit and Christensen, 2008.)

was discovered originally), but is not found globally. A typical flow velocity is 15 km yr^{-1} (0.5 mm s^{-1}).

Using this velocity estimate and the estimate for the internal field strength of the geodynamo from above, the magnetic energy density in the core is roughly three orders of magnitude larger than the kinetic energy density (although there is some uncertainty about the energy in small-scale components, in particular of the velocity field). This is in contrast to conditions in the convection zone of the Sun, where these two energy densities are comparable on average.

7.2.2.2 The Earth's paleofield

Most rocks contain small (sometimes minute) amounts of ferromagnetic minerals. A remanent magnetization can be acquired in various ways when a rock is formed. Of particular importance is the thermoremanence of a magmatic rock that cools in an ambient magnetic field below the Curie temperature (where a mineral becomes magnetic) and the blocking temperature (where the acquired magnetization becomes insensitive to later changes in field direction). From oriented and dated rock samples the field direction and sometimes the magnetic field strength at the time of their formation can be determined. This is not straightforward, because alterations of the rock at some later time may involve the formation of new ferromagnetic grains and lead to a "magnetic overprint". To unravel the magnetic palimpsest, each rock sample is stepwise demagnetized in the laboratory, by heating it up or by the application of an AC magnetic field. The resulting changes in the direction and intensity of the remanence signal are measured in order to retrieve the primary magnetization.

This technique and its refinements have been applied to rock samples of all ages and also to artifacts, such as potsherds, which provide more detailed information

for the past couple of thousand years. The oldest rocks that have been used for robust paleointensity measurements date back 3.2 billion years (Tarduno *et al.*, 2007). Although the intensity of the geomagnetic field fluctuates on various time scales, there is no long-term trend. For most of the time the intensity is found to be within a factor of two or three of the present field strength.

The detailed geometry of the field is more difficult to determine from paleomagnetic data, because the times of magnetization of samples from different locations are not synchronous. Furthermore, for rocks older than 5–10 million years continental drift becomes important, i.e. the location of the rock at the time when it was formed is not the same as it is today. In fact, the movements of the continents are calculated from paleomagnetic data under the assumption that the geomagnetic field is a geocentric axial dipole when averaged over long time intervals. Paleomagnetic data from the past 5 million years (for which the effects of continental drift are small) strongly support this hypothesis. The scatter found in these data, which is due to the combined influence of dipole tilt and of higher multipole contributions to the magnetic field, suggests that most of the time the amplitude of these two has been similar to what it is in the recent geomagnetic field. The dipole dominance is more difficult to prove for earlier times, but the available evidence is in support of it.

In summary, the Earth's magnetic field has not changed dramatically over the past three billion years in geometry or strength. A detailed account of our knowledge of the paleofield can be found in the book by Merrill *et al.* (1998).

7.2.2.3 Dipole reversals

One of the earliest findings by paleomagnetism is the occurrence of reversals of the dipole field. Today a detailed chronology of the geomagnetic polarity during the past couple of hundred million years has been established (Fig. 7.4 shows the past 120 million years). Compared to the length of periods with stable dipole polarity of some hundred thousand years, reversals are fairly rapid. The time interval during which the dipole axis is strongly tilted may last several thousand years. During reversals the dipole does not simply tip over, but also becomes much weaker, whereas the strength of higher multipole components does not seem to change much. Hence, the field at the Earth's surface becomes multipolar during a reversal. Aside from complete reversals, so-called geomagnetic excursions are also found in the paleomagnetic data. During these short events, the dipole axis becomes strongly tilted, often by more than 90°, but swings back to its original orientation.

On average, the geomagnetic field has reversed a few times in a million years during the recent geological past. In contrast to the cyclic behavior of the solar magnetic field, the timing of geomagnetic reversals is random: the probability of a reversal to occur is independent of the time that has passed since the last reversal. However, on time scales of 100 million years the reversal frequency itself

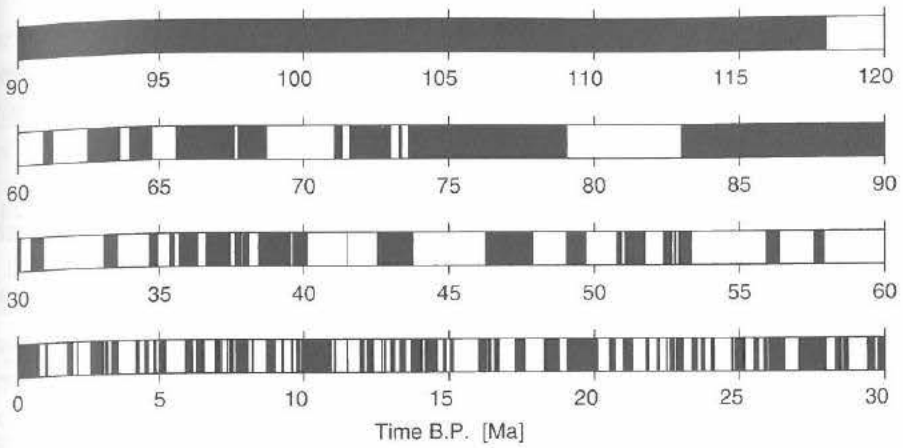

Fig. 7.4. Polarity of the geomagnetic field for the past 120 million years, with time running backward from left to right in each row (before present – BP, i.e. 1950 – in units of millions of years). Dark regions indicate times when the dipole polarity was the same as today, in white regions it has been opposite.

changes drastically. In a 35 million year time interval that ended 83 million years ago, the so-called Cretaceous superchron, no reversals occured at all. The reversal frequency increased gradually after the superchron, and decreased before the superchron. Other superchrons existed earlier in Earth's history, but are less well documented. The reversal frequency changes on a time scale that is comparable to the overturn time of the sluggish convection in the Earth's silicate mantle. For this reason it is assumed that the reversal frequency may be controlled by the slowly changing conditions in the lowermost mantle, for example its thermal structure, which would affect convection in the liquid core. Further details on reversals are found in Merrill *et al.* (1998) or Glatzmaier and Coe (2007).

7.3 Magnetic fields of other planets and satellites

The magnetic fields of all major planets in the solar system have been characterized by space missions during flybys or from orbiting spacecraft carrying vector magnetometers (Connerney, 2007; see Vol. I, Chapter 13 for a discussion of planetary magnetic fields and their associated magnetospheres). So far, this has provided only relatively crude snapshots in comparison to our knowledge of the geomagnetic field. Next to nothing is known about the time variability of the magnetic fields of planets other than Earth. In some cases the separation of internal (dynamo) and external (magnetospheric) contributions to the field observations is a significant source of uncertainty. Table 7.1 gives an overview on the field properties of the planets and some of their satellites.

Table 7.1. *Properties of magnetic fields of planets and satellites.*

Object	Active dynamo	R_c/R_p	B_{rms}[nT]	Dipole tilt	P_2/P_1	P_3/P_1
Mercury	Yes?	0.75	300	<5°?	0.1–0.5?	
Venus	No	0.55				
Earth	Yes	0.55	44 000	10.4°	0.04	0.24
Moon	No; yes in past?	0.2?				
Mars	No; yes in past	0.5				
Jupiter	Yes	0.84	640 000	9.4°	0.10	0.09
Ganymede	Yes	0.3	1 000	4°		
Saturn	Yes	0.6?	31 000	0°	0.02	0.22
Uranus	Yes	0.75	48 000	59°	1.3	1.5?
Neptune	Yes	0.75	47 000	45°	2.7	6?

Listed are the ratio R_c/R_p of the core to the planetary/satellite radius, the rms value B_{rms} of the surface magnetic field, the dipole tilt angle relative to the spin axis, and the ratios of quadrupole power or octupole power to the dipole power (P_2/P_1 and P_3/P_1) at the outer boundary of the dynamo at $r = R_c$. See Fig. 13.2 in Volume I for a graphical respresentation of the magnetic fields of the Earth and the giant planets.

Mercury The discovery of Mercury's internal magnetic field during a flyby of Mariner 10 in 1975 came as a surprise. Before then, it was believed that internal activity had ceased in the small planet. The flybys of the MESSENGER spacecraft in 2008 confirmed that the field is dominated by a dipole slightly tilted relative to the rotation axis. The relative importance of higher multipole contributions remains uncertain. The field strength at the planetary surface is $B_{rms} \approx 300\,\text{nT}$. Finding an explanation for this very low value, compared to those of other planets with a dynamo, is a challenge for the theory of planetary dynamos.

Venus No intrinsic magnetic field has been observed at Venus. The upper limit for the dipole moment is 10^{-5} of Earth's value. Unlike in the case of Mars (see below), a small-scale magnetic field due to remanent magnetization of crustal rocks that could be indicative for an ancient dynamo has not been observed either. However, the Venusian surface temperature of ~735 K is close to, or above, the Curie temperature of ferromagnetic minerals. Also, there is evidence that Venus' entire crust was renewed some 500 million years ago, which would have erased any magnetization that might have existed before. The answer to the question whether Venus once had an operating dynamo therefore remains elusive.

Moon The Earth's satellite has no global field at present. Small-scale magnetic fields that locally reach a strength of several tens of nT have been observed. Lunar rock samples brought to Earth by the Apollo missions show remanent magnetizations. The origin of the magnetization could be the field of an ancient dynamo, but

the small size of the lunar core and the associated geometric decrease of the field strength may be a problem. An alternative hypothesis for the acquisition of the magnetization involves strong local magnetic fields in the plasma clouds generated for a short time by big meteor impacts.

Mars Mars has no global magnetic field, but strong fields of crustal origin exist at the local or regional scale. Their amplitude is several hundred nT at a spacecraft altitude of 200 km, corresponding to probably several thousand nT at the Martian surface. This is considerably stronger than the magnetic field contribution from crustal magnetization on Earth. The only plausible cause for its acquisition is the existence of a strong global field generated by an early dynamo. Pronounced local fields are found in the very old southern highlands on Mars and are nearly absent in the younger northern lowlands. From the magnetization (or its absence) associated with large dated impact basins it has been estimated that the dynamo ceased to operate 4.1 billion years ago (i.e. around the time of the Late Heavy Bombardment, see Chapter 4).

Jupiter The detection of Jupiter's global magnetic field pre-dated the planet's exploration by spacecraft. It was inferred from the observation of strong emissions of radiowaves in the decameter wavelength range. These are generated by energetic electrons that gyrate around magnetic field lines close to Jupiter's surface (Barrow and Carr, 1992). Jupiter's field is about ten times stronger at the surface than the geomagnetic field, but the morphology is fairly similar: the dipole tilt is around ten degrees, and the ratios of the quadrupole and octupole components to the dominant dipole component are similar for both planets.

Saturn Saturn's field is slightly weaker at the surface than Earth's field. The dipole tilt is indistinguishable from zero. Furthermore, only zonal quadrupole and octupole components are needed in addition to the axial dipole to fit the field measurements by passing spacecrafts and the Cassini orbiter. This creates a problem for dynamo theory, because a strictly axisymmetric magnetic field cannot be generated by a dynamo according to Cowling's theorem (Section 4.1.5 in Vol. I).

Uranus and Neptune Uranus and Neptune can be dealt with jointly: their magnetic fields are similar to each other, yet distinct from those of other planets. So far, Uranus' and Neptune's fields have been characterised during a single flyby by Voyager 2 at each of these planets and uncertainties remain concerning details of the field structure. However, while the surface field strength is comparable to that at Earth, the geometry is clearly different. The dipole axis is strongly inclined with

respect to the rotation axis and quadrupole and probably octupole contributions are comparable to the dipole magnitude at the surface. At the probable radius of the top of the dynamo region, the quadrupole and octupole field are stronger than the dipole field (Table 7.1). While all other dynamo-generated planetary magnetic fields in the solar system are dipole-dominated, those of Uranus and Neptune must properly be termed multipolar.

Ganymede Jupiter's largest moon Ganymede is the only satellite in the solar system for which a global field with a probable dynamo origin has been found. Ganymede orbits inside Jupiter's magnetosphere and the strength of the Jovian field at Ganymede is about 120 nT, or one-eighth of Ganymede's intrinsic field. Other Jovian satellites have weak induced fields. The temporal change of Jupiter's field at the satellite position due to the rotation of the planet with its tilted dipole induces currents in the electrically conducting interior of the satellite. The strength of the induced field is at most comparable to that of the inducing field. Ganymede's field also has this component, but the surface field strength of 1000 nT is much larger than that of the Jovian field at this distance. The observations taken during repeated flybys of the Galileo spacecraft require a nearly axial dipole field that is intrinsic to Ganymede.

7.4 Structure and energy budget of planetary interiors

In this section the internal structure and the energy budget of planetary interiors are discussed as far as they are relevant for the operation of a dynamo. We distinguish between the rocky (terrestrial) planets of the inner solar system and the gas planets in the outer solar system. Both types of planets can host dynamos, although their structure and their energetics are different. A schematic overview of planetary internal structure is given in Fig. 7.5.

7.4.1 Earth

Earth serves as the prototype for the terrestrial planets. Its interior structure is known in some detail from seismology. Observations of the travel times of compressional waves and shear waves, and of frequencies of free oscillations of the Earth (which are excited by big earthquakes), can be inverted for the distribution of elastic properties and density inside our planet. There is a core with radius $R_c \approx 0.55 R_p$. Its outer part does not support the propagation of shear waves and hence is liquid. The small inner core, with a radius $R_{ic} = 0.35 R_c$, is clearly distinct. Since its discovery in 1935, it has been assumed to be solid. This is not

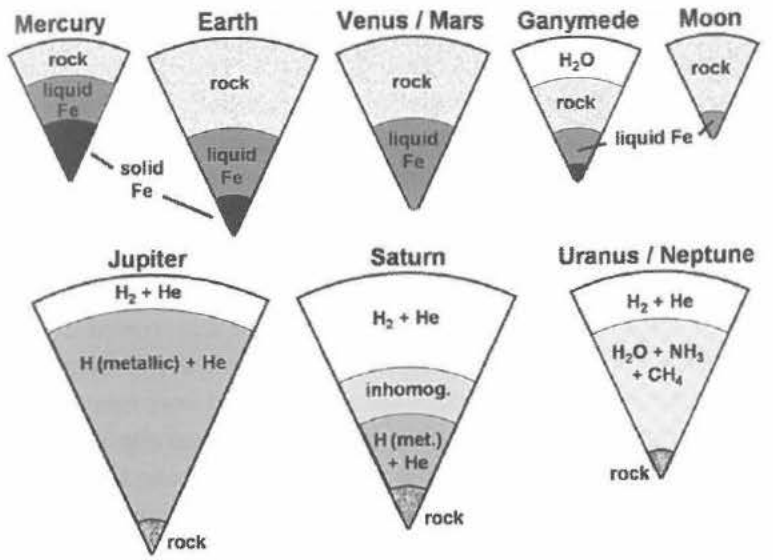

Fig. 7.5. Interior structure of planets with active or extinct dynamos. The top row shows the rocky (terrestrial) planets, and the bottom row the much larger gas planets. Larger planets are shown slightly larger, but relative sizes are not drawn to scale.

easy to prove, but from the observed frequencies of free oscillation modes that are particularly sensitive to the shear strength in the inner core, it has been made certain.

The core appears to consist predominantly of iron. Iron is the only element with sufficient cosmochemical abundance for which density and compressibility at the appropriate pressures and temperatures match the seismologically determined values of the core. Nickel also contributes, but is very similar in properties to iron. However, the density in the outer core is slightly less than that of pure iron–nickel and ~10% of a light chemical element must also be present. Silicon and oxygen are the top candidates, although others such as sulfur are likely to contribute. The composition of the solid inner core is closer to pure iron–nickel.

The total internal heat flow at the Earth's surface is 46 TW (although a large number, it is only 0.03% of the total power coming into the Earth's atmosphere by insolation). Roughly one-half of it is balanced by the heat generated by the decay of uranium, thorium, and the potassium isotope ^{40}K inside the Earth. The remainder of the heat flow is due to the cooling of the Earth. The loss of gravitational potential energy associated with the contraction of the Earth contributes a modest amount, but is much less important than it is in young stars or in gas planets. How much of the Earth's heat flow comes from the core is rather uncertain. Recent estimates that are based on different lines of evidence mostly fall into the range 5–15 TW

(Nimmo, 2007, Lay *et al.*, 2008), although values as low as 3–4 TW have also been discussed. Most of the radioactive elements reside in the silicate crust and mantle. Some potassium may be present in the core, but the majority of the core heat must be due to cooling. It is important to note that the heat loss from the core is regulated by the slow solid-state convection in the mantle. The core, which convects vigorously in comparison to the mantle and which is thermally well-mixed, delivers as much heat as the mantle is able to carry away.

Radiative heat transfer is not an issue in planetary cores, but liquid metal is a good thermal conductor. The heat flux that can be transported by conduction along an adiabatic temperature gradient, $(\mathrm{d}T/\mathrm{d}r)_{\mathrm{ad}} = T/H_T$, is sometimes called the "adiabatic heat flow" (T is absolute temperature, $H_T = c_p/(\alpha g)$ is the temperature scale height with c_p the heat capacity, α the thermal expansivity and g the gravitational acceleration). In terrestrial planets, the adiabatic heat flow can be a large fraction of the actual heat flow, or it may exceed the actual heat flow, in which case at least the top layers of the core would be thermally stable. Near the top of Earth's core approximately 3–4 TW can be conducted along the adiabat (Lay *et al.*, 2008), i.e. close to the minimum estimates for the entire core heat flow. But even if all heat flux near the core–mantle boundary were carried by conduction, a convective dynamo can exist thanks to the inner core. At the inner core boundary, the adiabatic temperature profile of the convecting outer core crosses the melting point of iron. The latter increases with pressure more steeply than the adiabatic gradient, which is the reason why the Earth's core freezes from the center rather than from above. As the core cools, the inner core grows with time by freezing iron onto its outer boundary. This has two important implications for driving the dynamo. The latent heat that is released upon solidification is an effective heat source, which contributes to the heat budget approximately the same amount as the bulk cooling of the core. The heat flux that originates at the inner core decreases with radius as r^{-2} in the spherical geometry of the fluid core. The adiabatic temperature gradient is roughly proportional to r, because gravity decreases towards the center. Therefore, even if the actual heat flux were slightly less than the adiabatic heat flux near the core–mantle boundary, it must be superadiabatic deeper down. A second, perhaps more important effect is that the light elements in the outer core are preferentially rejected when iron freezes onto the inner core. Hence, they become concentrated in the residual fluid near the inner core boundary. This layering is gravitationally unstable because of the reduced density, which leads to compositional convection that homogenizes the light elements in the bulk of the fluid core. Compositional convection contributes as much as, or more than, thermal convection to the driving of the geodynamo in recent geological times.

Most models for the inner core growth rate imply that the inner core did not exist for most of the history of the Earth. Rather, it would have nucleated between

0.5 and 2 billion years ago. In the absence of an inner core, only thermal convection by secular cooling of the fluid core (and perhaps radioactive heating) can drive a dynamo, which is less efficient than the present-day setting. A change in the geomagnetic field properties might be expected upon the nucleation of the inner core, but no clear indication for such an event has been found in the paleomagnetic record.

7.4.2 Other terrestrial planets

Few data are available to constrain the internal structure and thermal budget of terrestrial planets other than Earth (Sohl and Schubert, 2007; Breuer *et al.*, 2007). The mean density and the composition of surface rocks strongly suggest that they are differentiated into crust, mantle, and core, as is the case for Earth. The moment-of-inertia factor C/MR_{p}^2, where C is the polar moment of inertia and M the planetary mass, is sensitive to the radial variation of density inside the planet. Aside from Earth, the only other terrestrial planet for which it has been constrained so far is Mars, where it confirms the existence of a core. The observed reaction of Mars to solar tides shows that the core must be at least partially liquid. The observation of forced librations, i.e. slightly uneven rotation under the influence of a solar torque, suggests the same for Mercury. Because of Mercury's high mean density its core must be very large in relation to the size of the planet. However, the core radius cannot be constrained precisely in the cases of Mercury, Venus, Mars, and the Moon. A major source of uncertainty is the amount of light elements in the cores of these bodies.

No direct evidence on the existence or non-existence of a solid inner core is available for any planet other than Earth. But the possible absence of an inner core could explain why Venus and Mars do not have an active dynamo. On Earth mantle convection reaches the surface in the form of plate tectonics, which is a fairly efficient mode of removing heat from the interior. None of the other terrestrial planets have plate tectonics. In their cases, mantle convection is confined to the region below the lithosphere, a rigid lid of some 100–300 km thickness through which heat must be transported by conduction. Without plate tectonics, the heat flow is expected to be significantly lower not only at the surface, but also at the top of the core, where it is very probably subadiabatic. If no inner core exists to provide latent heat, it is then subadiabatic throughout the core. Furthermore, compositional convection is also unavailable to drive a dynamo. The slower cooling of the planetary interior in the absence of plate tectonics concurs with the idea that an inner core has not (yet) nucleated in the cases of Mars and Venus. Early in the planets' history the cooling rate was probably much higher and the associated core heat flow large enough for thermal convection. The demise of the dynamo

must have occurred when the declining heat flow dropped below the conductive threshold.

7.4.3 Gas planets

Jupiter and Saturn are similar in composition to the Sun (Guillot and Gautier, 2007). Shells of a hydrogen–helium mixture surround a small rocky core. In the outer envelope, where hydrogen forms H_2 molecules, the electrical conductivity is poor. At high pressure, hydrogen becomes a metallic liquid with free electrons (density is too high while temperatures are not high enough to call it a plasma). Shock-wave experiments show that there is no first-order phase transition, but the electrical conductivity rises gradually and reaches metallic values at around 1.3 Mbar pressure (Nellis *et al.*, 1999). This is reached at a depth corresponding to 84% of Jupiter's radius and 62% of Saturn's.

Uranus and Neptune also have an envelope rich in hydrogen and helium, but the bulk of their mass consists of a water-rich mixture of water, ammonia and methane, termed "ices" in planetology, even if in a fluid state (Guillot and Gautier, 2007). The ice layer extends to approximately 75% of the radius. It has ionic electrical conductivity, which is two orders of magnitude lower than the metallic conductivity in the cores of terrestrial planets and the large hydrogen planets, but probably sufficiently high to sustain a dynamo.

The internal heat flow of the gas planets has been determined by monitoring their infrared luminosity in excess of the re-emission of absorbed sunlight. The source of internal heat is mostly the potential gravitational energy lost upon contraction. The results of simple evolution models of the planetary interior agree with the observed luminosity of Jupiter, but underpredict it in the case of Saturn and overpredict it for Neptune and in particular for Uranus. The He/H-ratio in Saturn's atmosphere seems to be less than the solar ratio. Stevenson (1980) proposed that helium becomes immiscible with hydrogen in the upper part of the metallic layer in Saturn, resulting in a downward segregation in the form of a "helium rain". The gravitational energy of the ongoing internal differentiation boosts the luminosity to the observed value. The radial dependence of the helium depletion in the upper part of the metallic shell results in a stable compositional stratification which suppresses convection. For Uranus and Neptune it has been suggested that stratification in deeper parts of the ice layers inhibits convection and explains the reduced ability of these planets to lose internal heat.

The possible compositional stratification may impede convection in the electrically conducting cores of the outer planets, but thermal conduction along an adiabat is insufficient to transport the observed amounts of internal heat. In compositionally stratified regions the thermal gradient must be superadiabatic and unstratified layers should convect vigorously.

7.5 Some basics of planetary dynamos

Planetary dynamos share with stellar dynamos that the basic physical concept for their description is that of convection-driven magnetohydrodynamic flow in a rotating spherical shell combined with the associated magnetic induction effects. The principles of such dynamos have been discussed in detail in Chapter 6 and in Vol. I, Chapter 3, but here it is useful to recall some requirements and assumptions for planetary dynamos. Next, specific conditions for the magnetohydrodynamic flow in planetary cores are discussed; these flows are, for example, more strongly influenced by rotational forces than the flow in the solar convection zone.

Inside a shell of depth d with an electrical conductivity σ the fluid must move with a sufficiently large characteristic velocity v, so that the magnetic Reynolds number

$$R_\mathrm{m} = \frac{vd}{\lambda} \tag{7.3}$$

exceeds a critical value $R_{\mathrm{m,crit}}$ in order to have a self-sustained dynamo ($\lambda = 1/\mu_0\sigma$ is the magnetic diffusivity, with μ_0 magnetic permeability). The flow pattern must also be favorable for dynamo action, which requires a certain complexity. In particular, helical (corkscrew-type) motion with a large-scale order in the distribution of right-handed and left-handed helices is suitable. The Coriolis force plays a significant part in the force balance of the fluid motion and influences the pattern of convection. With this, the requirement for "flow complexity" seems to be satisfied and self-sustained dynamo action is possible above $R_{\mathrm{m,crit}} \approx 40$–$50$ (Christensen and Aubert, 2006).

At greater depth in the solar convection zone, the magnetic Reynolds number reaches values of order 10^9 for molecular values of the magnetic diffusivity (see appendix to Chapter 5). In the geodynamo R_m is approximately 1000. This fairly moderate value allows for the direct numerical simulation of the magnetic field evolution without the need to use an "effective diffusivity" or a parameterization of the induction process through a turbulent α-effect (Section 3.4.6 in Vol. I and Section 6.2.1). The ability to run simulations at the relevant value of R_m may be the most important cause for the success of geodynamo models.

The density in the Sun varies by many orders of magnitude with depth and the convection region spans many density scale heights. The density changes associated with radial motion are thought to be important. Flow helicity arises in the Sun because of the action of the Coriolis force on rising expanding and sinking contracting parcels of plasma (Section 5.2.4). Strong magnetic flux tubes have their own dynamics, because the reduction of fluid pressure that compensates magnetic pressure reduces their density and makes them buoyant (Section 5.4.3). In contrast, the dynamo region in Jupiter covers approximately one density scale height and it covers much less in terrestrial planets. The two compressibility effects

mentioned before probably do not play a significant role in planetary dynamos. Present geodynamo models usually neglect the small density variation and assume incompressible flow in the Boussinesq approximation (where density differences are only taken into account for the calculation of buoyancy forces).

Many models of the solar dynamo assume that most of magnetic field generation occurs at the tachocline, the shear layer between the radiative deep interior and the convection zone of the Sun (Section 5.5.5). For planetary dynamos the process of magnetic field generation is thought to occur in the bulk of the convecting layer.

The thinking on planetary dynamos has been shaped by the theory for the onset of rotating convection and by theoretical arguments on the dominant force balance for the flow in planetary cores (Jones, 2007). The relevant equation of motion for an incompressible fluid is

$$\rho\left(\frac{\partial \mathbf{v}}{\partial t}+(\mathbf{v}\cdot\nabla)\mathbf{v}\right)+2\rho\Omega\,\mathbf{e}_z\times\mathbf{v}+\nabla P=\rho\nu\nabla^2\mathbf{v}+\rho\alpha g T\,\mathbf{e}_r+\mathbf{j}\times\mathbf{B}, \quad (7.4)$$

where $\mathbf{v}$ is velocity, $\mathbf{e}$ a unit vector, Ω rotation rate, ρ density, P non-hydrostatic pressure, ν kinematic viscosity, α thermal expansivity, g gravity, T temperature, $\mathbf{B}$ magnetic field, $\mathbf{j}=\mu_0^{-1}\nabla\times\mathbf{B}$ current density, r radius, and z the direction parallel to the rotation axis. The terms in Eq. (7.4) describe, in order, the linear and non-linear parts of inertial forces, Coriolis force, pressure gradient force, viscous force, buoyancy force, and Lorentz force.

In the non-magnetic and rapidly rotating case, the primary force balance is between the pressure gradient force and the Coriolis force (geostrophic balance), similar to large-scale weather systems in the Earth's atmosphere. Ignoring all other terms in Eq. (7.4) and taking the curl, we arrive at the Taylor–Proudman theorem, which predicts the flow to be two-dimensional with $\partial\mathbf{v}/\partial z=0$. The only type of perfectly geostrophic flow in a sphere, i.e. a flow that satisfies this condition, is the differential rotation of cylinders that are co-aligned with the rotation axis (geostrophic cylinders). Such flow can neither transport heat in the radial direction, nor can it act as a dynamo. Convection requires motion away from and towards the rotation axis. This must violate the Taylor–Proudman theorem, because a column of fluid that is aligned with the z-direction will then stretch or shrink because it is bounded by the outer surface of the sphere. Hence the velocity cannot be independent of z. The necessity to violate the Taylor–Proudman theorem inhibits convection and requires that some other force, such as viscous friction, must enter the force balance. In order for viscosity to do so, the length scale of the flow must become small, at least in one direction. But the flow maintains a nearly geostrophic structure as far as possible. At the onset of convection it takes the form of columns aligned with the rotation axis (Fig. 7.6; see

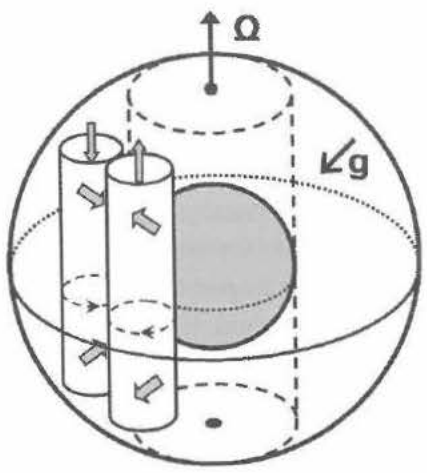

Fig. 7.6. Columnar convection in a rotating spherical shell near onset. The inner core tangent cylinder is shown by broken lines. Under Earth's core conditions the columns would be much thinner and very numerous.

also Section 5.2.4). They surround the inner core tangent cylinder like pins in a roller bearing. The tangent cylinder is parallel to the z-axis and touches the inner core at the equator. It separates the fluid core into dynamically distinct regions.

The primary circulation is around the axes of these columns. However, in addition there is a net flow along the column axes which diverges from the equatorial plane in anticyclonic vortices and converges towards the equatorial plane in columns with a cyclonic sense of rotation. The combination implies a coherently negative flow helicity in the northern hemisphere and positive helicity in the southern hemisphere. Busse (1975) demonstrated that this flow can serve as an efficient dynamo of the α^2-type (Section 3.4.6.2 in Vol. I).

When the motion becomes more vigorous at highly supercritical convection and when a strong magnetic field is generated, other forces such as inertia (advection of momentum) and the Lorentz force can affect the flow. However, one difference between the solar dynamo and planetary dynamos is the different role of inertial forces versus the Coriolis force. Their ratio is measured by the Rossby number

$$R_o=\frac{v}{\Omega\ell}, \quad (7.5)$$

where v and ℓ are characteristic velocity and length scales, respectively. Deep in the solar convection zone $R_o\approx 1$ when the pressure scale height is taken as ℓ. With typical estimates for the flow velocity in the Earth's core (1 mm s^{-1}), the Rossby number is of order 10^{-6} when a global scale such as the core radius or

shell thickness is used for ℓ. Therefore, fluid motion in the geodynamo is often considered to be largely unaffected by inertial forces. The general force balance is believed to be that between Coriolis force, pressure gradient force, Lorentz forces, and buoyancy forces (MAC balance = Magnetic, Archimedean, Coriolis; Roberts, 1987). However, at small scales inertial forces may become important also in planetary dynamos and can potentially feed back on the large-scale flow (see Section 7.6.2).

Like rotation, the presence of an imposed uniform magnetic field inhibits convection in an electrically conducting fluid. However, the combination of a magnetic field and rotation reduces the impeding influence that either effect has separately. This constructive interference is most efficient when the Coriolis force and the Lorentz force are in balance. For an imposed uniform field this is the case when the Elsasser number,

$$\Lambda = \frac{\sigma B^2}{2\rho\Omega}, \tag{7.6}$$

is of order one. For this force balance, called magnetostrophic, the flow pattern becomes large scaled. Applied to dynamos, it is argued that as long as the magnetic field is weak ($\Lambda \ll 1$), any field growth will intensify convection, meaning more efficient dynamo action and further increase of the field. Field growth at $\Lambda \gg 1$ would weaken convection, hence it is assumed that the field equilibrates at an Elsasser number of one. The field strength inside the geodynamo or in Jupiter's dynamo seems to agree with the Elsasser number rule (Stevenson, 2003). However, numerical dynamo simulations put some doubt on its validity (see Section 7.6.5).

A special condition applies to the integral force acting on geostrophic cylinders in the azimuthal direction. Buoyancy has no azimuthal component and the Coriolis force and the pressure gradient force are zero when averaged over the surface of these cylinders. If both viscous and inertial forces make a negligible contribution, the Lorentz force must also vanish, meaning that the magnetic field must maintain a special configuration. When this condition is satisfied, a dynamo is said to be in a "Taylor state". Disturbing the Taylor state will accelerate the cylinders, but the shearing of magnetic field lines penetrating neighboring cylinders, which is associated with the differential rotation, provides a restoring Lorentz force. The results are so-called torsional oscillations around the Taylor state, which in the Earth's core should have periods of some decades. Evidence for torsional oscillations has been claimed from fast secular variations of the geomagnetic field (Zatman and Bloxham, 1997). However, inertial effects of small-scale turbulent motion may contribute significantly to the acceleration of the cylinders, in which case the concept of a Taylor state is of limited value.

7.6 Numerical geodynamo models

7.6.1 Setup and parameters for geodynamo models

Most modern geodynamo models are direct numerical simulations of the equations for convective flow in the Boussinesq limit for a rotating spherical shell and of the magnetic induction equation (Christensen and Wicht, 2007). The equations are usually written in terms of non-dimensional variables and dimensionless control parameters. Here, we give them in the form used by Christensen and Aubert (2006):

$$\frac{\partial \mathbf{v}}{\partial t} + \mathbf{u}\cdot\nabla\mathbf{v} + 2\hat{\mathbf{z}}\times\mathbf{v} + \nabla P = E\nabla^2\mathbf{v} + R_\mathrm{a}^*\frac{\mathbf{r}}{r_\mathrm{o}}T + (\nabla\times\mathbf{B})\times\mathbf{B}, \tag{7.7}$$

$$\frac{\partial \mathbf{B}}{\partial t} - \nabla\times(\mathbf{v}\times\mathbf{B}) = \frac{E}{P_\mathrm{m}}\nabla^2\mathbf{B}, \tag{7.8}$$

$$\frac{\partial T}{\partial t} + \mathbf{v}\cdot\nabla T = \frac{E}{P_\mathrm{r}}\nabla^2 T, \tag{7.9}$$

$$\nabla\cdot\mathbf{v} = 0, \quad \nabla\cdot\mathbf{B} = 0. \tag{7.10}$$

Equation (7.8) is the magnetic induction equation, which results from Maxwell's equations and Ohm's law for a moving fluid (e.g. Roberts, 2007), and Eq. (7.9) describes advection and diffusion of thermal energy, as measured by temperature T. The four non-dimensional control parameters are the Ekman number, measuring the ratio of viscous forces to the Coriolis force

$$E = \frac{\nu}{\Omega d^2}, \tag{7.11}$$

a modified Rayleigh number, measuring the ratio of buoyancy forces to the impeding rotational forces

$$R_\mathrm{a}^* = \frac{\alpha g_\mathrm{o}\Delta T}{\Omega^2 d}, \tag{7.12}$$

and the two diffusivity ratios: the Prandtl number

$$P_\mathrm{r} = \frac{\nu}{\kappa}, \tag{7.13}$$

and the magnetic Prandtl number

$$P_\mathrm{m} = \frac{\nu}{\lambda}. \tag{7.14}$$

Here, g_o is gravity at the outer boundary, ΔT the (superadiabatic) temperature contrast and κ the thermal diffusivity. $\left(R_\mathrm{a}^*\right)^{1/2}$ is often called the convected Rossby number in the astrophysical literature. R_a^* is related to the conventional Rayleigh

Table 7.2. *Order of magnitude of dynamo control parameters and diagnostic numbers in the Earth's core and in planetary dynamo models.*

	Control parameters			
	$R_a^*/R_{a,c}^*$	E	P_m	P_r
Earth's core	~5000	10^{-15}–10^{-14}	10^{-6}–10^{-5}	0.1–1
Models	1–1000	10^{-3}–10^{-6}	0.1–10^3	0.1–10^3
	Diagnostic numbers			
	R_m	R_e	R_o	Λ
Earth's core	~10^3	~10^9	~10^{-5}	0.1–10
Models	50–3000	10–2000	3×10^{-4}–10^{-1}	0.1–100

Listed are the modified Rayleigh number (Eq. 7.12), relative to the critical value for the onset of convection in the absence of a magnetic field, the Ekman number E (Eq. 7.11), the magnetic Prandtl number P_m (Eq. 7.14), the Prandtl number P_r (Eq. 7.13), the magnetic Reynolds number R_m (Eq. 7.3), the Reynolds number $R_e \equiv vd/\nu$, the Rossby number R_o (Eq. 7.5), and the Elsasser number Λ (Eq. 7.6). For comparison with values of the Prandtl, Reynolds, and Rossby numbers in the solar interior, see Table 5.1.

number $R_a = \alpha g_o \Delta T d^3/(\nu\kappa)$ by $R_a^* = R_a E^2 P_r^{-1}$. Equations (7.7)–(7.10) must be completed by appropriate boundary conditions. For Earth's core, impenetrable rigid boundaries with imposed constant temperatures or heat flux are usually taken. The magnetic field must match with an appropiate potential field outside the dynamo region.

In Table 7.2 we compare control parameter values used in geodynamo models with those for the Earth's core. The Rayleigh number has been normalized to its critical value $R_{a,c}^*$ for the onset of convection in the absence of a magnetic field. We also list several other non-dimensional numbers that are diagnostic for the dynamo and result from the model solution.

While the Prandtl number in the models is of the right order, the values of the other control parameters are far off. The Ekman number and the magnetic Prandtl number are too large in the models by factors of 10^{10} and 10^6, respectively. The modified Rayleigh number is too small with respect to supercriticality, but its absolute value is larger than the core value. In terms of physical parameters, the viscosity and thermal diffusivity are too large by a factor of order 10^6 compared to the magnetic diffusivity, which is about right. In addition, the rotation rate is too small by a factor of ~10^4 in most models. The magnetic Reynolds number R_m agrees with Earth values at least in the more advanced models, whereas the hydrodynamic Reynolds number $R_e = vd/\nu$ is far too small and the Rossby number R_o

is too large. The Elsasser number Λ can be taken as a non-dimensional measure for the magnetic field strength. The claim that a model reproduces the geomagnetic field strength actually means that it has an Elsasser number of order one.

Because of the large discrepancies in some of the control parameters it has been suspected that the dynamical regime in the models is different from that in planetary dynamos and that the agreement in the magnetic field properties found in some of them is fortuitous. In particular, viscosity might play an important role in the models whereas it is insignificant in the Earth's core.

7.6.2 Types of dynamo solutions

Many published geodynamo models have a magnetic field on the outer boundary that is strongly dominated by the axial dipole. Often the dipole in such models shows no tendency to ever reverse, although the model run time may not have been long enough to capture one of these rare events. Other numerical dynamos have a multipolar field, which is in many cases spatially complex without any obvious symmetries and is rapidly varying in time. The two classes of solution are rather distinct and few in-between cases have been found. Figure 7.7 shows examples of the two types. The underlying models are "advanced" in the sense that the Ekman number is decently small (from the point of numerical feasibility) and the magnetic Reynolds number is Earth-like in both cases. The spatial power spectrum at the outer boundary of the dynamo models is typically fairly white for harmonic degrees from 3 to 13, but in one class of solutions the dipole stands above the higher multipoles, as it does in the power spectrum of the geomagnetic field at the core–mantle boundary (Fig. 7.1), whereas it falls below the multipole level in the other class. In the fully developed multipolar regime the weak dipole component changes its polarity continuously in an erratic way.

Systematic model studies suggest that the ratio of inertial forces relative to the Coriolis force plays a key role for the selection of the magnetic field geometry. When inertia is weak, the field is very dipolar. When inertia becomes relevant, the dynamo switches to generating a multipolar field. The Rossby number (Eq. 7.5) calculated with the shell thickness is still significantly smaller than unity in the multipolar cases; for example in the models shown in Fig. 7.7 it is 0.01 and 0.02, respectively. Christensen and Aubert (2006) suggested that a "local" Rossby number is a more appropriate measure for the ratio between inertial forces and the Coriolis force:

$$R_{ol} = \frac{v}{\Omega \ell}. \tag{7.15}$$

The mean flow length scale ℓ is taken from the kinetic energy spectrum as function of wavelength. Analyzing a large number of model results, Christensen and

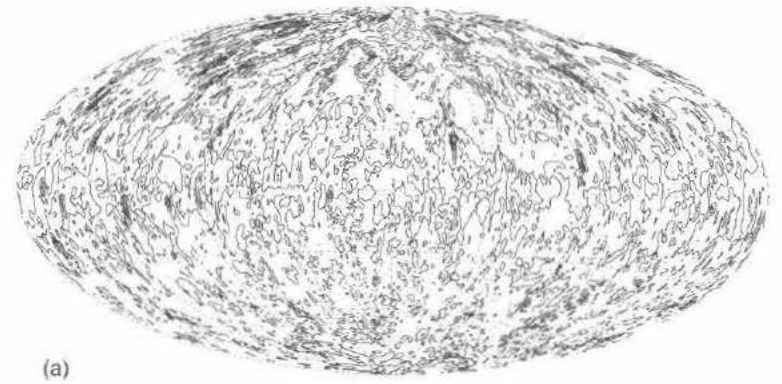

(a)

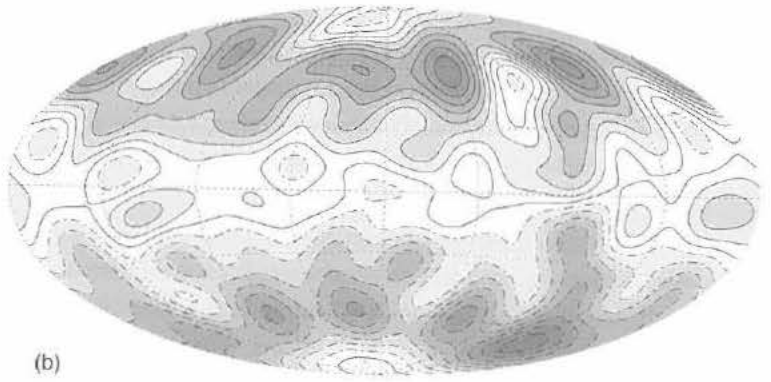

(b)

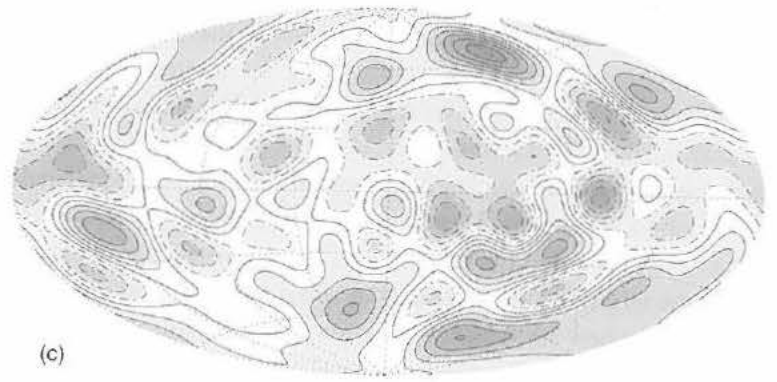

(c)

Fig. 7.7. Snapshots of the radial magnetic field component on the outer boundary from numerical dynamo models. Solid lines are used for outward flux and dashed lines for inward flux (arbitrary contour steps in each panel). Grey scale indicates absolute amplitude. (a) Model parameters $E = 10^{-5}$, $R_a^* = 0.12$, $P_m = 0.8$, $P_r = 1$. (b) Same field low-pass filtered to harmonic degrees $n < 14$. (c) Model parameters $E = 10^{-5}$, $R_a^* = 0.17$, $P_m = 0.5$, $P_r = 1$, low-pass filtered. R_m is approximately 900 in both cases; R_{ol} is 0.125 in (a) and (b), and 0.19 in (c). See Color Plate 4.

Aubert (2006) found that a transition from dipolar to multipolar magnetic field occurs when R_{ol} exceeds a critical value of approximately 0.12, irrespective of what the values of control parameters such as E, P_r, and P_m are. Dipolar dynamos that show occasional reversals have a local Rossby number near the transitional value. Hence a reversal may represent an accidental brief lapse of the basically dipolar dynamo into the multipolar regime. When the dipole recovers, it can then take either polarity.

Olson and Christensen (2006) derived an empirical rule based on numerical model data for relating the local Rossby number to the fundamental control parameters of the dynamo. It involves powers of all four control parameters and requires an extrapolation over a large range to apply it to the planets. Nonetheless, using appropriate parameter values for the Earth, $R_{ol} \approx 0.1$ is predicted for the geodynamo, which puts it close to the transition point between the dipolar and the multipolar class, in agreement with the occasional occurrence of reversals. One problem is that the flow length scale associated with this value of R_{ol} is only $\ell \approx 100$ m. Even if eddies of such size have significant energy in the core, at this scale the magnetic field is diffusion-dominated and cannot be affected directly by the flow. An indirect effect is conceivable. For two-dimensional turbulence it is well known that small scales transport energy into large flow scales ("inverse cascade", e.g. Davidson, 2004). The nearly geostrophic flow at the onset of rotating convection is quasi-two-dimensional. In the dynamo models the flow is still preferentially aligned with the axis of rotation. If this is also the case in the Earth's core, small eddies may affect the circulation at large scales and play a direct role in the induction process.

7.6.3 Flow structure and field generation mechanism

The stretching of magnetic field lines by differential rotation in the case of the solar dynamo, particularly at the tachocline, is thought to be of major importance for the generation of a toroidal magnetic field that is much stronger than the poloidal field (Section 5.4.3). In most geodynamo models, in contrast, differential rotation does not contribute much to the total kinetic energy and the toroidal and poloidal magnetic field components have similar strength. As mentioned before, the flow is strongly organized by rotational forces and the vortices are elongated in the z-direction. Even at a highly supercritical Rayleigh number and in the presence of a strong magnetic field, the flow outside the inner-core tangent cylinder is reminiscent of the helical convection columns found at onset. Inside the tangent cylinder, the flow pattern is different and often exhibits a rising plume near the polar axis (Fig. 7.8b). The plume is accompanied by a strong vortex motion (called a "thermal wind") with a retrograde sense of rotation near the outer surface changing to

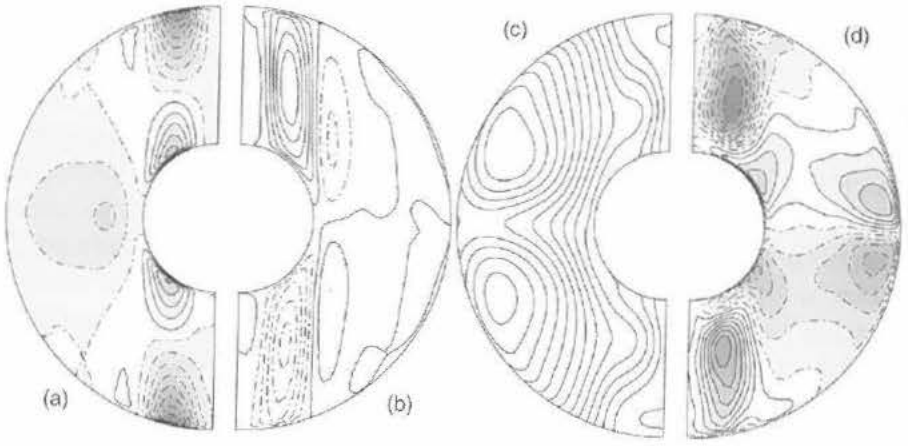

Fig. 7.8. Time-averaged axisymmetric components of velocity and magnetic-field components for a planetary dynamo model with $R_a^* = 0.225$, $E = 3 \times 10^{-4}$, $P_r = 1$, $P_m = 3$. $R_m \approx 250$ and $R_{ol} \approx 0.1$. The grey scale indicates absolute intensity. (a) Azimuthal velocity, broken lines are for retrograde flow, (b) streamlines of meridional velocity, full lines for clockwise circulation, (c) poloidal magnetic field lines, (d) azimuthal (toroidal) magnetic field, broken lines westward directed field.

prograde rotation at depth (Fig. 7.8a), because the Coriolis force acts on the associated converging flow near the inner core boundary and diverging flow near the outer boundary.

Several authors have analyzed their numerical dynamo solutions in order to understand the basic mechanism by which the magnetic field is maintained. In the tradition of mean-field dynamo theory it is considered how large-scale (e.g. axisymmetric) poloidal field is converted to large-scale toroidal field and vice versa. There is general agreement that the axial dipole field is generated from the axisymmetric toroidal field by an α-effect associated with the helical flow in the convection columns outside the tangent cylinder. In mean-field theory as it is used in astrophysics, the α-effect is associated with unresolved turbulent eddies (Vol. I, Section 3.4.3). In the geodynamo models a "macroscopic" α-effect is observed.

The mechanism for generating the axisymmetric toroidal field is less clear and both an α-effect and differential rotation (Vol. I, Sections 3.3.7 and 3.4) seem to play a role. Often two flux bundles in the azimuthal direction are found outside the tangent cylinder, with opposite polarity north and south of the equatorial plane (Fig. 7.8d). Olson *et al.* (1999) show that they are generated from the axisymmetric poloidal field by a similar macroscopic α-affect associated with the helical convection columns (α^2 dynamo). Other authors show that the Ω-effect (the shearing of poloidal field by differential rotation) contributes strongly to the generation

of axisymmetric toroidal field, even though the kinetic energy in the differential rotation is rather limited. While in weakly driven numerical dynamo models the regions inside the tangent cylinder, north and south of the inner core, are nearly quiescent, vigorous flow is found here in more strongly driven models. In these cases a strong axisymmetric toroidal field is found inside the tangent cylinder region, produced by the shearing of poloidal field lines in the polar vortex (Fig. 7.8a, c, d).

7.6.4 Comparison of geodynamo models with Earth's field

Some criteria to judge the similarity between the magnetic field of a dynamo model and the geomagnetic field are (1) the agreement in field strength, (2) the agreement in the shape of the spatial power spectrum, (3) qualitative agreement in the magnetic field morphology, (4) an agreement in the time scales of secular variation, and (5) agreement in the frequency and characteristic properties of dipole reversals. Many published models do well with respect to some of these criteria and a few satisfy most of them to a fair degree. A good guide for a dynamo model to generate an Earth-like magnetic field is probably that the magnetic Reynolds number and the local Rossby number must assume the appropriate values. Other parameters may be less critical. We defer the discussion of the field strength to Section 7.6.5 and address the other criteria below.

The shape of the geomagnetic power spectrum up to degree 13 at the core–mantle boundary (Fig. 7.1) is reproduced rather well by several models, although often the dipole is somewhat stronger or weaker relative to higher multipoles than in the present geomagnetic field (see Christensen and Wicht, 2007, for more details). Comparing Figs. 7.2b and 7.7b, similar morphological structures are found. The model reproduces flux lobes at high latitudes, which are roughly aligned on similar longitudes in both hemispheres, although they may be more numerous than they are in the geomagnetic field. The model also shows weak flux at the poles and scattered flux spots of both polarities at low latitudes.

The cause for these various magnetic structures in the core field has tentatively been inferred from the flow structures that are predicted by theory and seen in the dynamo models (Gubbins and Bloxham, 1987; Christensen *et al.*, 1998). The high-latitude flux concentrations are related to the helical convection columns outside of the inner core tangent cylinder. Cyclonic vortices are associated with downflow near the surface (Fig. 7.6) that concentrates magnetic flux. Low flux at the poles can be related to the upwelling plume near the rotation axis which disperses magnetic field lines. The variation of the geomagnetic field in the north polar region of the core–mantle boundary, assuming that it is frozen into the fluid, also supports the existence of an anticyclonic vortex motion near the core–mantle

boundary, which should accompany the rising plume (Olson and Aurnou, 1999; Hulot *et al.*, 2002).

Finally, bipolar pairs of flux spots at low latitudes are found in many dynamo models. They have been associated with the emergence of toroidal magnetic flux tubes through the core–mantle boundary, analogous to the mechanism for the formation of bipolar active regions on the Sun (Christensen *et al.*, 1998, Christensen and Olson, 2003). The pairs are often north–south rather than east–west aligned and their polarity is opposite to the global dipole polarity. Such a configuration arises in the models because strong toroidal fields of opposite polarity are found at close distance north and south of the equator (Fig. 7.8d) and because the columnar flow is north–south aligned and acts on both toroidal tubes in the same way. Comparable structures exist in the Earth's field at the core–mantle boundary (see Fig. 7.2b, beneath Africa and the Atlantic Ocean) and have been explained by flux expulsion (Bloxham, 1989). However, in the geomagnetic field they are more strongly offset from the equator than they are in dynamo models and overall the semblance between model field and geomagnetic field is less convincing regarding the low-latitude flux spots than it is for other magnetic structures.

Matching the time scales of secular variation is a matter of magnetic Reynolds number. For Earth-like values of R_m the model magnetic field changes at the observed rates, provided model time is scaled to real time using the magnetic diffusion time scale d^2/λ. There is a certain circularity in this argument, because the magnetic Reynolds number of Earth's core is estimated under the assumption that most of the observed secular variation is due to the frozen-flux advection of magnetic structures.

Geodynamo models that are in the right regime for dipole reversals often show a degree of agreement with the paleomagnetic record that goes beyond the simple occurrence of reversals, even in cases with very modest parameter values such as a relatively large Ekman number. Figure 7.9 shows time series of the dipole tilt, dipole moment and relative dipole field strength in such a model. Some of these properties resemble traits of the geomagnetic field: (1) the directional change of the dipole field is a relatively brief event compared to the length of the period in which the dipole is nearly aligned with the rotation axis; (2) the dipole moment starts to drop before the directional change occurs, and during the reversal the magnetic field is multipolar; and (3) apart from complete reversals, strong changes occur in the dipole direction that are brief and non-persistent (geomagnetic excursions). The actual frequency of reversals in geodynamo models seems to depend on the fine tuning of parameters. The search for a clearly defined "mechanism" for reversals in the dynamo models has not yet come up with a unique answer.

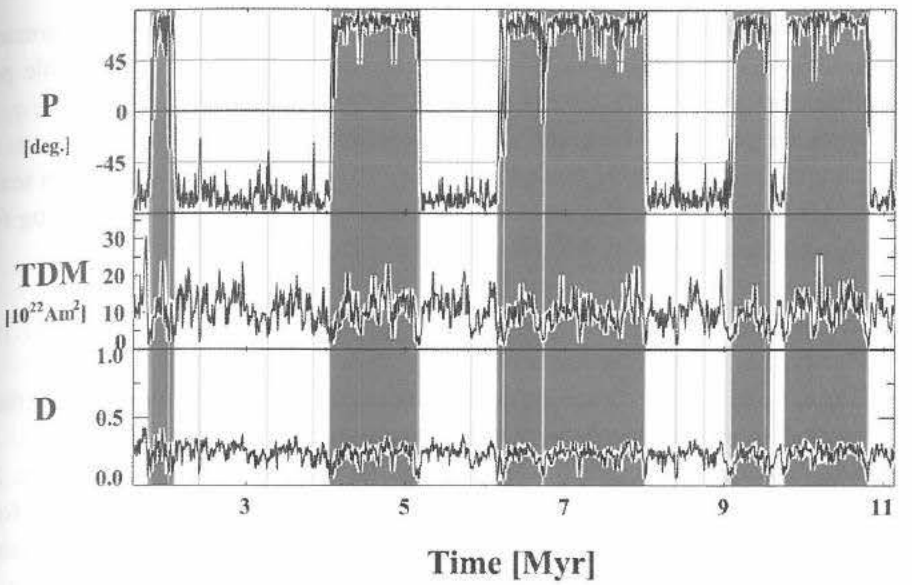

Fig. 7.9. Evolution of the dipole tilt for a modeled planetary magnetic field with respect to the equator (P), the true dipole moment (TDM), and the dipole strength relative to the total field strength at the core–mantle boundary (D) for a dynamo model with $E = 10^{-3}$, $R_a^* = 0.5$, $P_m = 10$, $P_r = 1$. The present TDM of the geomagnetic field is 8×10^{22} A m^2. Dark and light bands indicate polarity intervals. (From Christensen, 2009, courtesy of Johannes Wicht.)

7.6.5 Scaling of magnetic field strength

Dynamo scaling laws relate characteristic properties, for example the mean magnetic field strength, to fundamental quantities of the planet and its core, such as core radius R_c, density ρ, conductivity σ, rotation rate Ω, and convected energy flux q_c. As explained in Section 7.5, it has commonly been assumed that the magnetic field strength in a planetary dynamo is determined by a magnetostrophic force balance. Magnetostrophic balance is often associated with an Elsasser number of order one, which means that the magnetic field strength scales as $B \propto (\rho\Omega/\sigma)^{1/2}$. Notably, the Elsasser number is independent of the energy flux. Stevenson (1983) pointed out that this scaling is unlikely to be universally applicable, because it ignores the requirement that sufficient energy must be available for balancing Ohmic dissipation. Alternative scaling laws based on a magnetostrophic balance, which make different assumptions on how the Lorentz force depends on characteristic properties than those used for deriving the Elsasser number, have also been proposed (e.g. Starchenko and Jones, 2002).

Christensen and Aubert (2006) and Christensen *et al.* (2009) suggest that the magnetic field strength is not determined by a force balance, but solely by the

energetics of the dynamo, at least in rapidly rotating cases with a dipole-dominated magnetic field. For a thermally driven dynamo, the heat flux that is available per unit volume for conversion to other forms of energy is given by $H_T^{-1} q_c$, where q_c is the convected part of the heat flux and H_T is temperature scale height. The rate at which magnetic energy is dissipated scales as $\lambda B^2/\ell_B^2$, where ℓ_B is the length scale of the field. Equating energy generation and dissipation, the following scaling for the magnetic energy density is obtained:

$$\frac{B^2}{2\mu_o} \propto f_{\rm ohm} \frac{\ell_B^2}{\lambda} \frac{q_c}{H_T}, \tag{7.16}$$

where $f_{\rm ohm}$ is the fraction of the energy dissipated by Ohmic dissipation rather than by viscous dissipation. It is thought to be close to one in planetary dynamos.

The magnetic length scale ℓ_B depends on the magnetic Reynolds number. At high R_m the folding of field lines in the flow can continue to smaller scales before reconnection occurs. The flow velocity and hence R_m depend on the available energy flux as well. Here, we consider the scaling law based on this concept in the form proposed by Christensen *et al.* (2009), without going into the intricate scaling arguments that can lead to it:

$$\frac{B^2}{2\mu_o} = c\, f_{\rm ohm}\, \bar{\rho}^{1/3} (F q_o)^{2/3}, \tag{7.17}$$

where $\bar{\rho}$ is the mean density, c is a constant prefactor, q_o a reference value for the heat flux (for example the surface flux) and F is a dimensionless efficiency factor of order one. The necessary averaging of radially varying quantities, such as ρ, q_c or H_T, is condensed into the efficiency factor, which can be calculated for a given planetary or astrophysical object from a structural model and assumptions on the radial distribution of the convected flux. A remarkable point about Eq. (7.17) is that it predicts the surface-averaged magnetic field strength (or flux density) to be independent of rotation rate and of electrical conductivity. There are obvious limits to that; for example, for very low conductivity the magnetic Reynolds number would be subcritical and the field strength must be zero.

A fairly large number of geodynamo calculations are currently available that cover a decent range of the numerically accessible control parameter space. This allows scaling laws to be tested. Non-dimensionalizing Eq. (7.17) by dividing it by $\bar{\rho}\Omega\lambda$ leads to a non-dimensional energy flux q^* and a scaled magnetic energy density that is identical to the Elsasser number $E_m^* = \Lambda$. The dependence on density drops out in the non-dimensional form of Eq. (7.17). Figure 7.10 compares E_m^* to the right-hand side of the non-dimensionalized Eq. (7.17) for dynamo simulations with a dipolar magnetic field. The efficiency factor F, which results from the model setup, has been calculated analytically. The fraction of Ohmic dissipation has been

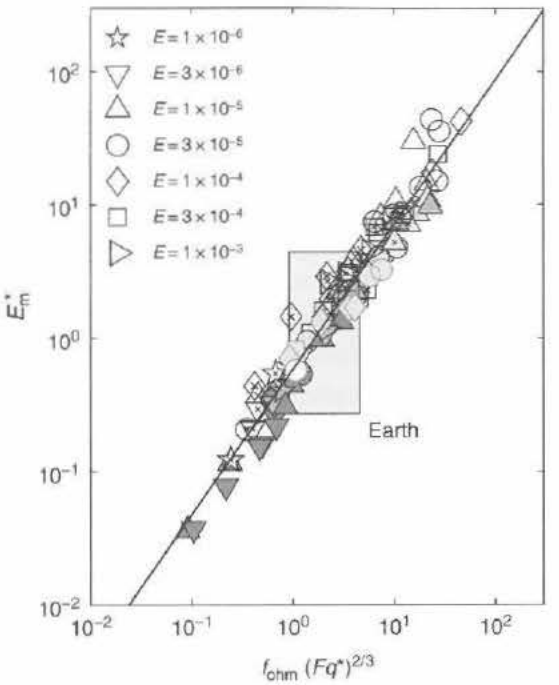

Fig. 7.10. Non-dimensional magnetic energy density in numerical dynamo models versus 2/3-power of the non-dimensional available energy flux. Symbol shape indicates Ekman number (Eq. 7.11), shading of the symbols magnetic Prandtl number (Eq. 7.13); darker means a lower value. Crosses inside the main symbols indicate $P_r > 1$ and circles indicate $P_r < 1$. Symbols with black edges are models driven by an imposed temperature contrast, those with grey edges are for compositional convection. The line represents the fit for a forced slope of one, equivalent to an exponent of 2/3 in Eq. (7.17). The location of the geodynamo in the diagram is shown by the grey rectangle.

recorded for each dynamo run, where it is typically in the range 0.3–0.8. While the exponents in Eq. (7.17) come from scaling theory, the prefactor $c = 0.63$ is obtained by fitting the numerical model results.

Figure 7.10 shows a number of important points. (1) The Elsasser number is not always close to unity in the different dynamo models, but varies over three orders of magnitude. (2) The model results fall on a single line reasonably well, irrespective of the value of Ekman number (which differs by three orders of magnitude) and of the two Prandtl numbers (which differ by two orders of magnitude each between different models). The Ekman and Prandtl control parameters describe the influence of viscosity, magnetic, and thermal diffusivity, and of the rotation rate. Therefore, these quantities do not play an important role in the field strength. The fear that the dynamical regime in the models differs fundamentally from that

in the Earth's core (and could be dominated by viscosity) is probably unfounded. (3) The model results agree reasonably well with the 2/3-power scaling law. A best fit results in a slightly larger exponent of 0.71. (4) The magnetic field inside Earth's core (estimated to be in the range 1–4 mT) agrees well with the prediction for current estimates of the heat flow at the core–mantle boundary and the associated compositional driving due to inner core growth (grey rectangle in Fig. 7.10).

To estimate the magnetic field strength inside the dynamos of other planets, the observed (low-order) magnetic field must be downward continued to the outer boundary of their dynamo region and an assumption must be made on the factor by which the internal field is stronger, which is guided by the ratios found in the numerical dynamo models. Jupiter's field strength agrees well with the prediction (Fig. 7.11). Other solar system bodies are more problematic. For Mercury

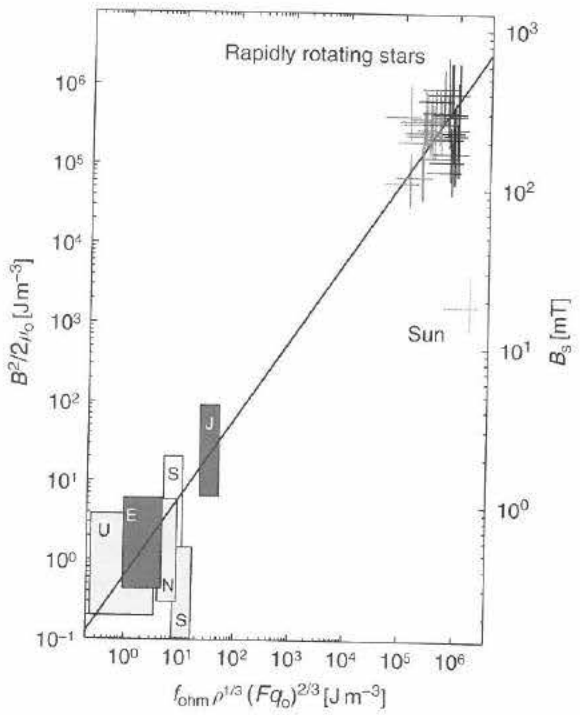

Fig. 7.11. Magnetic energy density in the dynamos of planets and certain stars versus the predicted dependence on a function of available energy flux and density. E: Earth; J: Jupiter; S: Saturn; U: Uranus; N: Neptune. The grey rectangle for Saturn is for a dynamo boundary at $0.62R_p$ and the white rectangle for $0.4R_p$. Black crosses for rapidly rotating main-sequence stars of low mass and grey crosses for classical T Tauri stars. The scale on the right is the average field strength (or flux density) at the surface of the dynamo. The black line is taken from Fig. 7.10 and converted here to physical units.

and Ganymede the available energy flux is very uncertain. The strengths of the multipolar fields of Uranus and Neptune may not fall on the line that has been calibrated with dipolar dynamo models, although within the uncertainties it seems to be compatible. Saturn's field is too weak for a dynamo that extends to the top of the metallic hydrogen layer at approximately 60% of the planetary radius. If the top of the active dynamo region, below a stably stratified region, is put at $0.4R_p$, the result can be brought into line with the prediction (compare Sections 7.4.3 and 7.7.3).

Is the scaling law applicable to other convection-driven spherical dynamos in cosmic bodies? The solar dynamo seems fundamentally distinct from the dynamos of Earth or Jupiter, because the Sun rotates too slowly and/or because of the special role played by the tachocline in the field generation process. Main-sequence stars with less than 0.35 solar masses (M-type dwarfs) are fully convective, and so are very young contracting T Tauri stars (see Chapters 2 and 3). Hence, they lack a tachocline. Furthermore, these stars generally rotate much more rapidly than the Sun does. The rapid rotators have strong surface magnetic fields in the range of several tenths of a tesla (several kilogauss). Recent observational evidence shows that the magnetic flux of M-type dwarfs increases with decreasing rotation period (decreasing Rossby number) up to some threshold, but becomes independent of rotation rate for the more rapidly rotating stars (Reiners *et al.*, 2009; compare Section 2.3.2). This is akin to the independence of the field strength on rotation rate found in the numerical geodynamo models. Furthermore, the mapping of the magnetic field topology of some mid-M dwarfs by a technique called Zeeman–Doppler tomography shows strong large-scale magnetic field components at the surfaces of these objects, which are often dominated by the axial dipole (see Section 2.6 and Fig. 2.16; also, e.g. Morin *et al.*, 2008).

Christensen *et al.* (2009) found that the observed magnetic flux density of rapidly rotating M-type dwarf stars and of T Tauri stars agrees with the prediction of Eq. (7.17), as shown in Fig. 7.11. The slowly rotating Sun does not fall on the same line. Note that the solid line in the figure is *not* a fit to the various objects, but both its slope and the prefactor c have been taken from scaling theory and from the fit to the results of numerical geodynamo models shown in Fig. 7.10. The fact that rapidly rotating stars fall on the same line as the planets strongly supports the validity of the scaling law. Furthermore, it suggests that dynamos in rapidly rotating stars are not fundamentally different from planetary dynamos, despite the much higher energy flux and far greater magnetic Reynolds number.

A more detailed account on scaling laws for planetary dynamos, including the scaling of velocity and ohmic dissipation is found in Christensen (2009).

7.7 Dynamo models for Mercury and the gas planets

Existing dynamo models for planets other than Earth are derivatives of geodynamo models, where some parameter or other has been adapted to the assumed conditions in the specific planet. This does not concern the fundamental control parameter – they cannot be made to match planetary values anyway. Several of these models assume the existence of stably stratified layers in the fluid core of the planet.

7.7.1 Mercury

The main task of a dynamo model for Mercury is to come up with an explanation for the weakness of the observed magnetic field. Stevenson (1987) suggested that the flow in Mercury's core would be too slow for the magnetic Reynolds number to exceed the threshold of a standard hydromagnetic dynamo, but that a "thermoelectric" dynamo may generate the observed weak field. Topography on Mercury's core–mantle boundary would imply slight variations of its temperature. These are accompanied with spatial differences of the thermoelectric EMF arising from the contact of two different materials. The associated currents would set up a toroidal magnetic field (that is invisible from outside). The α-effect of helical flow in Mercury's core acting on this toroidal field would generate poloidal field even at modest values of R_m. Conditions for this model to work are that the lower mantle of Mercury is a fairly good conductor, so that the thermocurrents can close, and that the core topography is of large scale, in order to explain the large-scale external field. It is highly uncertain whether these conditions are met.

Mercury probably has a solid inner core. Its size is very uncertain, but may be quite large, with only a thin fluid shell remaining. Some thin-shell dynamo models (Stanley *et al.*, 2005, Takahashi and Matsushima, 2006) succeeded in producing relatively weak magnetic fields outside the dynamo region. However, these fields are either still too strong by a factor of ten or more, or they are rather multipolar, in contrast to the observed dipole dominance.

The outer part of Mercury's fluid core is probably stably stratified, because thermal conduction along a distinctly subadiabatic temperature gradient is sufficient to carry the expected modest core heat flow. A deep sub-shell of the fluid core might then convect, driven by the latent heat of freezing of the inner core and the associated light element flux. Christensen (2006) and Christensen and Wicht (2008) presented numerical dynamo simulations for such a scenario and found that in the dynamo layer a strong magnetic field is generated. Mercury's slow rotation with a period of 59 days implies that the local Rossby number is larger than one. Consequently, the internal dynamo field is small scaled, not dipolar. The small-scale field varies rapidly with time. Therefore, it is strongly attenuated by a skin effect in the conducting stable layer above the dynamo and is virtually unobservable outside of the core. The dipole component makes only a small contribution inside the dynamo, but it varies more slowly with time. Hence, it can penetrate through the stable layer to some degree and dominates the structure of the very weak field at the planetary surface. Some of these models match the observed field strength and geometry.

Mercury's magnetosphere is very small (see Vol. I, Chapter 13). At the top of Mercury's core the external field created by the magnetospheric current systems is much stronger relative to the internal field than it is in case of the Earth. Glassmeier *et al.* (2007) suggest that the feedback of the external field may play an important role for the dynamo. Including it in a kinematic $\alpha\Omega$ dynamo model, they find two branches of solution, with a strong and a weak magnetic field, respectively, of which the latter might represent the situation at Mercury. The hypothesis needs to be tested in MHD dynamo models.

7.7.2 Jupiter

The semblance in the geometry of Jupiter's field to that of the Earth's field and the finding that the field strength of both planets is well explained by the energy flux rule (Section 7.6.5) suggest that Jupiter's dynamo and the geodynamo are generically very similar. Some potentially important differences may exist, however. Unlike in the case of the Earth, where the electrical conductivity changes abruptly at the core–mantle boundary, in Jupiter it varies more gradually in the transition region between molecular and metallic hydrogen. An open question is whether the strong zonal wind circulation that is seen at Jupiter's surface is deep-rooted in the molecular hydrogen envelope, and if so, how it interfaces with the dynamics of the dynamo region. Other differences are that the radial density variation in Jupiter's metallic hydrogen shell is more pronounced than it is in the Earth's core and that the flow in Jupiter's dynamo is not strongly driven from below. Dedicated MHD simulations for Jupiter's dynamo are underway. NASA's foreseen Juno mission will characterize Jupiter's magnetic field with a much better resolution than was possible up to now. Having a closer look might reveal some significant differences from the geomagnetic field.

7.7.3 Saturn

The challenge in the case of Saturn's dynamo is to explain the high degree of axisymmetry of the magnetic field. The only conceptual model so far is that by Stevenson (1980, 1982), who suggested that the hypothetical stable layer, caused by the helium immiscibility in the upper part of the metallic hydrogen shell, plays the essential role. The density stratification suppresses convection, but is

still compatible with toroidal flow, such as differential rotation. Let us assume for simplicity that the whole stable layer rotates like a uniform shell with respect to the underlying dynamo region and that the dynamo field is stationary. Seen from a reference frame that is fixed to the rotating shell, the non-axisymmetric field components is time dependent, whereas the axisymmetric part is stationary. If the magnetic Reynolds number characterizing the shell motion is large enough, a skin effect eliminates the non-axisymmetric parts of the field, but leaves the axisymmetric components unaffected.

In this concept the role of the stable conducting layer, which shields the dynamo, is somewhat akin to that in the Mercury model by Christensen (2006). Differences are that in the Saturn case the primary dynamo field is dipolar because Saturn is a rapid rotator and that motion in the stable layer is important. Christensen and Wicht (2008) find in their dynamo models with a dipole-dominated field that latitudinal differences in the heat flux from the dynamo region into the overlying stable shell drive strong differential rotation as a thermal wind circulation. The magnetic field has significant non-axisymmetric components inside the dynamo region, but the field outside the core is very axisymmetric. The axisymmetry becomes much less when in a control experiment differential rotation in the stable layer is suppressed. These full MHD dynamo simulations support Stevenson's concept.

7.7.4 Uranus and Neptune

In the case of Uranus and Neptune it must be explained why their dynamos generate a multipolar field. Both planets rotate rapidly and the estimate by Olson and Christensen (2006) for the local Rossby number would put them into the dipolar regime. Either the local Rossby number rule for the selection of the field morphology fails, or the dynamos in these two planets are rather distinct from the geodynamo. Stanley and Bloxham (2004, 2006) present a dynamo model with a thin convecting shell that surrounds a conducting, but convectively stable, fluid core region. Some of their dynamo models generate magnetic fields that agree well with the spectral power distribution in the lower-order harmonic field components. It is also not clear if the much lower electrical conductivity in the interior of Uranus and Neptune, compared to that of other planetary dynamos, plays a role. Gómez-Pérez and Heimpel (2007) suggest that a less dipolar field may result in this case.

7.8 Outlook

Recent decades have been an exciting time for planetary magnetism. In addition to better characterizing the geomagnetic field in space and time, the exploration of the magnetic fields of other planets has brought some surprises. There is more

diversity than previously thought. At the same time, dynamo theory has matured, and modeling by direct numerical simulation is now feasible.

Geodynamo models are remarkably successful in reproducing many observed properties of the geomagnetic field. In this respect, planetary dynamo modeling seems to be more advanced than that of the solar dynamo. To some extent the task is easier for the geodynamo – our ignorance of the small-scale structure of the geomagnetic field implies that a model can be declared successful when it captures the crude properties. Our conceptual understanding of how exactly the geodynamo works has not quite kept pace with the modeling attempts. The reasons for the success of geodynamo models are a matter of speculation, but the following points may be essential: (1) It is possible to fully resolve the magnetic field structure and hence the details of the magnetic induction process. Put differently, direct numerical simulations at the correct value of the magnetic Reynolds number are feasible. (2) Although the model viscosity and thermal diffusivity are far larger than realistic microscopic values, they seem low enough to not alter the dynamical regime. (3) The flow at large and intermediate scales, which is responsible for magnetic induction, may be realistic in the model. This is made possible because rotation has a stronger influence than it has on the flow in the solar convection zone and imposes some order on the circulation. Also, the strong radial differences of density in the solar convection zone, which lead to large variations in length scales and velocity scales, are not a problem in planetary dynamos.

Future work on the geodynamo must improve our understanding of what the essential conditions are for an Earth-like model. The validity of the proposed scaling laws in a parameter range closer to Earth must be tested in simulations at lower values of the Ekman number and magnetic Prandtl number and in laboratory dynamo experiments. Their theoretical foundation must be put on firmer ground.

Dynamo models for explaining the magnetic fields of planets other than Earth have had some successes, too, but progress here is hampered by our very rudimentary knowledge of the relevant conditions inside these bodies. Cosmic objects such as rapidly rotating low-mass stars may provide a bridge between planetary dynamos and the solar dynamo. Modeling studies of convection-driven dynamos in a wide range of objects, together with improvements of our knowledge of their magnetic field properties from observation, may ultimately lead to a unifying dynamo theory explaining the commonalities and differences found in all these various objects.